Powder Technology 360 (2020) 1271–1277

Contents lists available at ScienceDirect

Powder Technology

journal homepage: www.elsevier.com/locate/powtec

Atomic force microscopy to identify dehydration temperatures for small volumes of active pharmaceutical ingredients

Katherine Atamanuk [a], Myles C. Thomas [b], Robert C. Wadams [b], Will Linthicum [a], Weili Yu [b,*], Bryan D. Huey [a,*]

[a] University of Connecticut, Department of Materials Science and Engineering, Storrs, CT 06269, United States of America
[b] Pfizer Global Research Laboratories, Drug Product Development, Groton, CT 06340, United States of America

ARTICLE INFO

Article history:
Received 8 April 2019
Received in revised form 13 September 2019
Accepted 14 September 2019
Available online 16 September 2019

Keywords:
AFM
Indentation
Dehydration
Hydrate
Anhydrous
Pharmaceutical

ABSTRACT

The environmental conditions associated with changing the hydration state of active pharmaceutical ingredients (API) are crucial to understanding their stability, bioperformance, and manufacturability. Identifying the dehydration event using < 1 μg of material is an increasingly important challenge. Atomic Force Microscopy indentation mapping is implemented at controlled temperatures between 25 and 100 °C, for nanoscale volumes of hydrated APIs exhibiting distinct dehydration behavior and anhydrous APIs as controls. For caffeine hydrate and azithromycin dihydrate, the relative mechanical modulus increases ~10-fold at dehydration temperatures. These are confirmed by conventional macroscopic measurements including Variable Temperature Powder X-ray Diffraction, Thermogravimetric Analysis, and Differential Scanning Calorimetry. Conversely, no such mechanical transition is observed for anhydrous ibuprofen or a proprietary anhydrous compound. AFM-based mechanical mapping is therefore demonstrated for small-volume determination of temperature-induced solid-state dehydration events, which may enable spatial or temporal mapping for future studies of dehydration mechanisms and kinetics as a function of commercially relevant nanoscale heterogeneities.

1. Introduction

Many active pharmaceutical ingredients (APIs) can exist in either anhydrous or hydrated crystalline forms. The impact of a change in the hydration state has been well studied and reported in the pharmaceutical literature [1–3]. Crucially, for a given API molecule, the hydrate and anhydrous forms can exhibit significantly different physical and chemical properties that can impact the stability, bioperformance, and manufacturability of the API and correspondingly the pharmaceutical product. Consequently, understanding and control of the hydration state is a crucial component of pharmaceutical development.

The most common factors that impact the hydration state of API powders are temperature and humidity. Characteristic of many hydrates is the dehydration temperature, the temperature above which a hydrated crystalline form loses water from its crystalline lattice, and transitions to a lower-order hydrate, an anhydrous crystalline form, or an amorphous form. Measuring such dehydration temperatures is most commonly achieved experimentally with Differential Scanning Calorimetry (DSC), Thermogravimetric Analysis (TGA), and/or Variable Temperature Powder X-ray Diffraction (VTPXRD) [4]. These macroscopic techniques typically require a minimum of a few milligrams (or roughly 0.005 mm^3) of API, and result in dehydration events occurring over a broad temperature range. Such observations are generally attributed to the comparatively large volume sampled by the experimental method with respect to the underlying physical mechanisms [5]. For instance, a wide thermodynamic transition can result from subtle variations in composition down to the nanoscale. Kinetic control may also contribute to, or even dominate, the measured specimen transition. This could result from many types of local microstructural variations, including grain size and orientation, crystallographic density, relative porosity, phase purity, amorphous content, the corresponding surface energies and concomitant hydrophilicity-hydrophobicity, surface morphology, and geometry such as core-shell configurations. Moreover, drug formulations increasingly leverage the high release rates of nanoparticulate APIs, where the enhanced surface to volume ratio can further amplify such effects. It is therefore crucial to develop small-volume or surface sensitive approaches for assessing critical physical properties of APIs and related polymer or biochemical systems to fundamentally investigate local thermodynamics and kinetics. More specifically for the pharmaceutical industry, drug discovery is consistently accelerating, which necessitates early detection and determination of key physical attributes with “miniaturized” API specimens to meaningfully influence early stage drug development, when available API quantities are scarce.

Atomic Force Microscopy (AFM) is a particularly well-developed tool for probing material properties at the nanoscale [6]. It is typically used to map the morphology of specimen surfaces, but more advanced

* Corresponding authors.
E-mail addresses: Weili.yu@pfizer.com (W. Yu), Bryan.Huey@UConn.edu (B.D. Huey).

https://doi.org/10.1016/j.powtec.2019.09.045
0032-5910/

modes employ the sharp and finely controlled tip to assess a wide variety of local materials properties [7]. Relevant to this study is the use of AFM for mechanical property measurements, especially via nanoindentation [7]. As indicated in Fig. 1A, a spherical tip is displaced towards, indented into, and then withdrawn from a surface via a z-oriented piezoelectric scanner. This causes the integrated cantilever to deflect, according to Hooke's law, towards or away from the surface for attractive or repulsive forces, respectively (Fig. 1B). With appropriate calibration, this behavior can resolve the local Young's modulus, adhesion force, and adhesion energy. Using arrays of such measurements on several APIs, these mechanical properties have been mapped for a range of controlled specimen temperatures via an integrated heater and thermocouple.

Four model systems are specifically investigated in this work. Caffeine, for example, generally wakes up approximately 64% of American adults [8], and has a reported dehydration temperature of ~51.5 °C [2]. Azithromycin, an antibiotic prescribed to treat bacterial infections, undergoes a two-step hydrous/anhydrous transition over a relatively broad temperature range around 80 °C [1]. Measurements from ibuprofen and a proprietary crystalline, anhydrous API are also reported, as these specimens do not exhibit a hydrate-anhydrous transition, and therefore serve as negative controls. For each of these specimens, local AFM based indentation measurements reveal marked increases in surface stiffness only at temperatures corresponding to dehydration according to supporting macroscopic measurements. This approach is therefore promising for investigations of hydration/dehydration events with API's and more broadly for other fundamental and applied studies with small volumes of crystalline materials.

2. Experimental section

2.1. Materials

Two hydrated model compounds are selected for this work, caffeine hydrate and azithromycin dihydrate. Anhydrous caffeine acquired commercially from SAFC is slurried in distilled water to form caffeine hydrate crystals. It is reported that caffeine hydrate is not a rigorous monohydrate but a 0.8 hydrate [2] or can also be classified as a non-stoichiometric hydrate [9]. Azithromycin dihydrate (Alembic Limited) is used as received. Two anhydrous materials are used in this work for comparison purposes. Anhydrous crystalline ibuprofen (Sigma Aldrich) was commercially acquired and a proprietary anhydrous crystalline drug (Compound A) was obtained from Pfizer development laboratories. The hydration state of the caffeine hydrate and azithromycin dihydrate are confirmed using powder X-ray diffraction. All specimens were sealed and stored at ambient temperature until needed for local or macroscopic experiments.

2.2. Variable temperature powder X-ray diffraction (VTPXRD)

Variable Temperature PXRD experiments are conducted with a commercial diffractometer (Bruker AXS D8 Advance) equipped with a Cu radiation source, operating with an X-ray tube voltage and amperage of 40 kV and 40 mA, respectively. Data is collected from 3.0 to 40.0° 2θ, in 0.03 2θ increments at a scan speed of 0.5 s per step. Samples are prepared by placing about 15–30 mg of sample in a silicon, low-background sample holder. Samples are heated from RT to the desired temperatures with a ramp rate of 1 °C/min and are held at each temperature for 30 min to allow for equilibration before x-ray analysis.

2.3. Differential scanning calorimetry (DSC)

DSC measurements are performed with a Discovery DSC (TA instruments) equipped with a refrigerated cooling accessory. All of the experiments are performed in standard aluminum pans. The cell constant is determined using indium and temperature calibration is performed using indium and tin as standards. All of the measurements are done under continuous dry nitrogen purge (50 mL/min). Approximately 3–5 mg of solid sample are weighed into aluminum pans in an open pan configuration. The samples are initially cooled to −40 °C for a stable baseline and then heated to melt at a rate of 1 °C/min.

2.4. Thermogravimetric analysis (TGA)

TGA analysis is conducted using a Discovery TGA (TA instruments) thermogravimetric analyzer. Samples of approximately 10 mg are weighed into aluminum pans and heated from ambient to 300 °C at 10 °C/min heating rate under nitrogen purge.

2.5. Atomic force microscopy (AFM)

Local mechanical measurements are achieved with Atomic Force Microscopy, using a standard commercial AFM instrument (Asylum Research MFP-3D). Each API specimen is mounted onto a steel disk that is magnetically attached to a sample heater (Asylum PolyHeater) connected to an external thermal controller, enabling programmable fixed or ramped temperatures. The AFM probes are optimized for indentation measurements on relatively compliant specimens, featuring a 2.5 μm radius silica glass sphere attached to the end of a cantilever (AppNano FORT SiO_2-A-5). The AFM system calibration remained consistent within better than 4% for all temperatures, established at each temperature using standard procedures. This includes pressing the probe into a relatively incompressible surface (the steel sample mount) to determine the system sensitivity ('inverse optical lever sensitivity'), and then measuring the thermal response of the cantilever near resonance from which the lever spring constant is calculated via the well-established Sader method [10]. An array of 16 × 16 force curves are then acquired, sampling a 2 × 2 μm^2 area, requiring 8 min for all 256 indentations. Samples are always heated with a ramp rate of 1 °C/min, comparable to the standard ramp rate for more macroscopic measurements. The peak temperature investigated is 93 °C. All measurements are repeated at least three times per temperature, for improved statistics and to minimize any effects of tip-sample geometry-related artifacts at any one area, yielding dehydration temperature results that are replicable within ±3 °C.

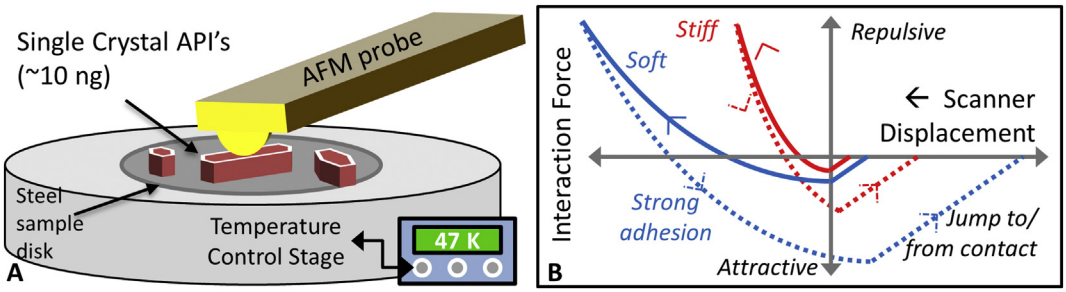

Fig. 1. Experimental schematic (A) and representative AFM indentation results (B).

Overall, this work is based on approximately 16,000 AFM indentations. For each, the bulk modulus and related mechanical measurements are calculated programmatically using commercial software (Mathworks Matlab). As diagrammed in Fig. 1B, when the tip indents into the sample, a force-distance loading curve is acquired. The local topography is determined from the scanner displacement necessary to reach a set-point repulsive force as if performing standard contact-mode AFM imaging, here 5 nN. The slope of the approach curve is then used to calculate the elastic properties of the sample according to the widely employed Hertzian model [11]. This method (Eq. (1)) relates localized stresses during contact between two surfaces and the corresponding sample deformation, with the force (F) proportional to the indentation (z) to the $^3/_2$ power for a hemispherical indentation profile as is applicable here.

$$F = \frac{4}{3} E^* R^{*\,1/2} z^{3/2} \tag{1}$$

The slope ($\partial F / \partial z^{3/2}$) is determined with a least squares fit between forces ranging from 75 nN to a peak force of 125nN. For rough surfaces on the scale of the tip apex the specimen curvature must also be incorporated, but in this case the samples are relatively planar so the reduced radius (R^*) is mathematically approximated by the large radius of the spherical commercial probes (2.5 μm). The local reduced modulus (E^*) is thereby determined, which accounts for the mechanical properties of both the relatively stiff probe apex and the comparatively compliant sample.

Finally, the sample modulus is calculated from Eq. (2), where ν_{tip} and E_{tip} are the Poisson's ratio and Young's modulus for the tip, while ν_{sample} and E_{sample} are the corresponding terms for the sample. The value of the tip Poisson's ratio and modulus are approximated for silica glass to be 0.19 and 68.0 GPa, respectively. The Poisson's ratio of the sample is not calculated but assumed to be 0.33 as widely employed for similar circumstances [12].

$$\frac{1}{E^*} = \left[\frac{\left(1-\nu_{tip}^2\right)}{E_{tip}} + \frac{\left(1-\nu_{sample}^2\right)}{E_{sample}} \right] \tag{2}$$

Each force-volume map of 16 × 16 indentations therefore provides maps of the height (Fig. 2A) and up to 256 modulus values (Fig. 2B). The moduli calculated for some locations yield non-physical solutions so are not considered further (black pixels in the maps of Fig. 2). For all samples and all temperatures studied, the maximum standard deviation per 16 × 16 pixel map ranges from 8 to 31% of the detected value. This signifies that the results are relatively homogeneous over the investigated 4 μm^2 field of view. Although not shown for brevity, the standard deviation for each modulus measurement (pixel) is also determined, based on the root mean squared (RMS) difference between the measured forces as a function of indentation and those expected according to the calculated modulus. This local standard deviation, as a percentage of the locally calculated modulus, is typically <3%.

Since a large diameter sphere is used to probe the specimen mechanical properties, and the samples are assumed to be relatively homogeneous, the results are primarily analyzed as histograms instead of

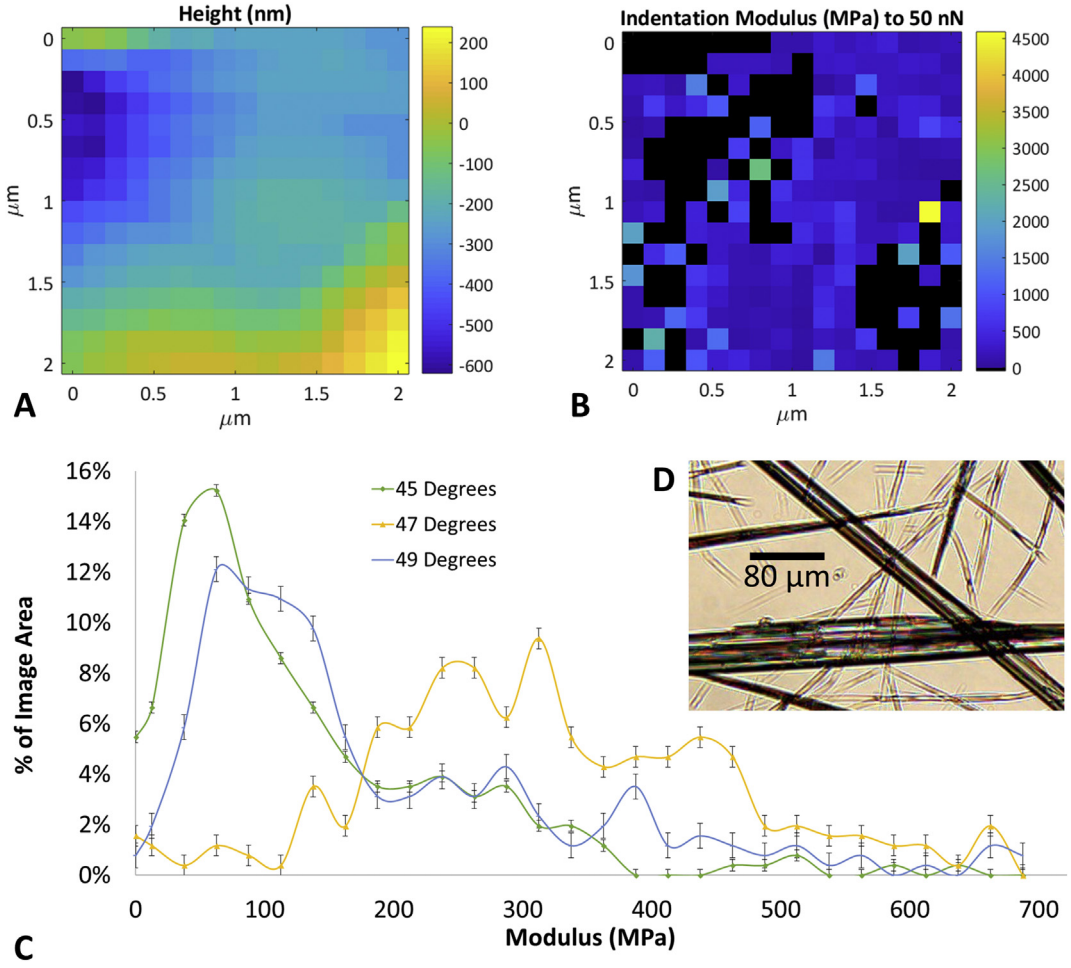

Fig. 2. AFM-based indentation procedure, including mapping the (A) height and (B) calculated modulus, (C) a histogram of these modulus results from similar measurements acquired at 3 critical temperatures, and (D) a representative optical micrograph of the most challenging of the specimens, i.e. the high aspect ratio caffeine hydrate single crystals.

maps. As an example, Fig. 2C presents the distribution of moduli measured for 3 distinct specimen temperatures for caffeine, where a shift in distribution occurs macroscopically near 50 °C. Specifically, the mode of the moduli distribution (peak in each histogram) shows a marked increase in the range of detected moduli for 47 °C. Such measurements are repeated for each specimen over a range of temperatures to assess whether the surface mechanical properties accessible via AFM couple to dehydration events. A micrograph of the caffeine hydrate, acquired at room temperature, is included in Fig. 2D and is structurally unchanged over the entire temperature range according to equivalent images acquired with an in-situ hot-stage. The micrograph is representative of this most complex of all of the specimens we studied, due to the typically high aspect ratios and range of diameters (5 to 50 μm) present for the caffeine single crystals.

3. Results and discussion

Dehydration events of caffeine hydrate and azithromycin dihydrate are first examined using conventional macroscopic (bulk powder) techniques, including Variable Temperature Powder X-Ray Diffraction (VTPXRD), Differential Scanning Calorimetry (DSC), and Thermal Gravitational Analysis (TGA).

Fig. 3A presents PXRD patterns of the caffeine sample obtained with increasing temperatures. The pattern obtained at room temperature is consistent with caffeine hydrate, showing characteristic diffraction peaks (*) at 10.5° 2Θ and 13.05° 2Θ [13]. As the temperature is increased to approximately 45 °C, a new diffraction peak (#) characteristic of anhydrous caffeine develops at approximately 11.7° 2Θ [14]. With rising temperature, intensity of characteristic hydrate peaks decreases while that of the anhydrous peak grows as caffeine hydrate continuously dehydrates. The hydrate peaks are undetectable at 55 °C indicating completion of the dehydration process.

Fig. 3B shows PXRD patterns of the azithromycin sample collected across a temperature range of 25 °C to 130 °C. The diffraction pattern collected at 25 °C is consistent with azithromycin dihydrate, showing characteristic peaks (*) at approximately 9.3° 2Θ and 9.8° 2Θ [1]. The diffraction patterns remain unchanged from 25 °C to 60 °C. At 70 °C, a new diffraction peak (#) begins to appear at 10.6° 2Θ. The new peak is characteristic of either the azithromycin anhydrate, or an isomorphic sesquihydrate according to Sundaramurthi et al [1]. By approximately 100 °C the dihydrate peaks are no longer detectible indicating completion of the dehydration process attainable under the experimental conditions. Some peak-broadening is present at 120 °C indicating development of disorder in the crystalline lattice with a complete melt observed at approximately 130 °C. Based on Sundaramurthi et al., heating of azithromycin dihydrate may first yield the sesquihydrate, which subsequently dehydrates to an isomorphic anhydrous form before becoming amorphous or melting. Due to the isomorphism, it is difficult to discern the temperature at which the sesquihydrate converts to anhydrate via VTPXRD alone.

Results of the DSC analyses of caffeine hydrate and azithromycin dihydrate are given in Fig. 4A. A broad endothermic peak reflecting the dehydration process of caffeine hydrate starts from room temperature and ended at approximately 80 °C. The DSC trace continues to decline after dehydration likely due to sublimation of anhydrous caffeine followed by the melting endotherm centered around 200 °C (marked as T_m). The lower onset temperature of dehydration comparing to that observed with the VTPXRD (~45 °C) is most likely due to the continuous dry nitrogen purge applied during DSC measurement. Caffeine hydrate is known to dehydrate at ambient temperature when relative humidity is below ~68% [5]. Under dry nitrogen purge, the relative humidity in the

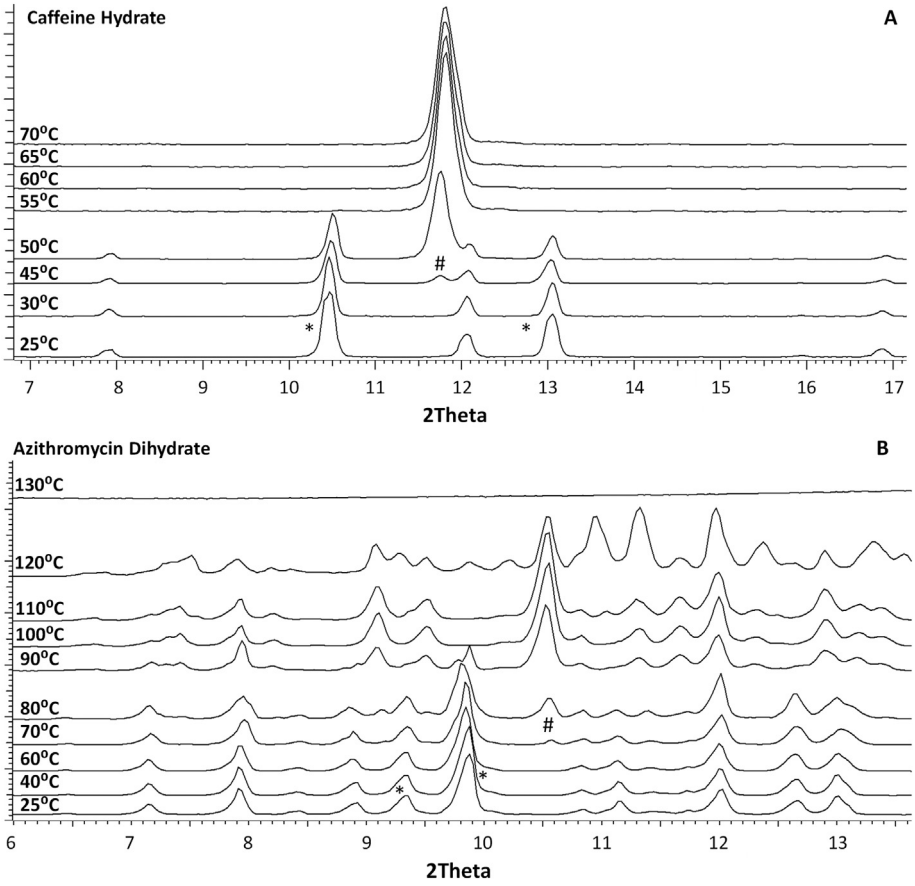

Fig. 3. VTPXRD diffraction upon heating approximately 15–30 mg of API to identify dehydration events of (A) Caffeine hydrate and (B) azithromycin dihydrate. Peaks marked with (*) denote characteristic peaks of the hydrated starting materials; peaks marked with (#) denote characteristic peaks of the anhydrous form after dehydration.

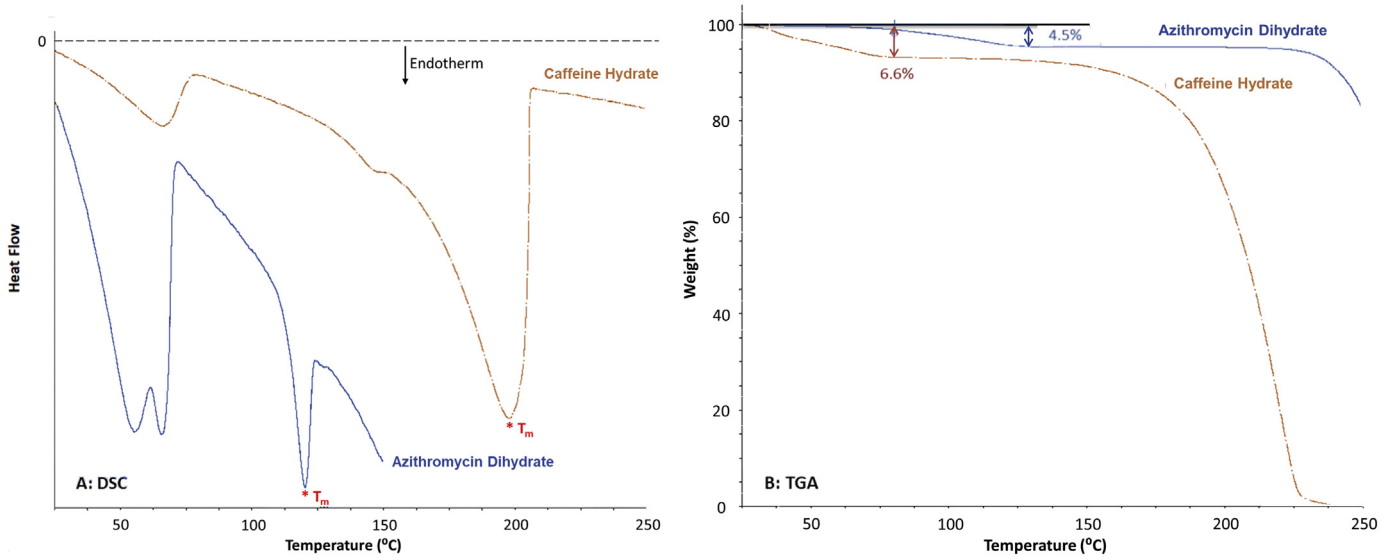

Fig. 4. (A) DSC with 3–5 mg of sample for caffeine hydrate and azithromycin dihydrate as labelled. Melting events of the anhydrous form of caffeine and azithromycin are marked as T_m. (B) TGA using 5–10 mg of samples for caffeine hydrate and azithromycin dihydrate. Weight loss of both samples indicates complete dehydration upon heating before melting.

DSC sample chamber is significantly below 68%, which leads to lower dehydration temperature as the sample is measured in an open-pan configuration. In comparison, the VTPXRD experiment is conducted under ambient relative humidity with no dry nitrogen purge applied. In addition, the difference in the onset dehydration temperature may also be caused by other experimental factors, such as the smaller sample mass used in DSC than VTPXRD.

A split in the broad endothermic peak is observed when the azithromycin dihydrate is heated from 25 °C and to 75 °C at a ramp rate of 1 °C/min. It is plausible that the split in the peak is resulted from the two-step dehydration process reported by Sundaramurthi et al., where the azithromycin dihydrate first converts to a sesquihydrate which subsequently dehydrates to an isomorphic anhydrate. A melt endotherm is observed at around 125 °C (marked as T_m), consistent with what is observed with VTPXRD. Similar to the case of caffeine hydrate, dehydration of azithromycin dihydrate begins at a much lower temperature during the DSC measurement due to the continuous purge of dry nitrogen, and the open pan configuration used for the study. While DSC is widely used to assess the dehydration temperature of hydrated systems, these examples clearly show that the temperature range for dehydration obtained from DSC can be very broad and highly dependent on experimental conditions, which may not always represent relevant storage and processing conditions of interest.

Thermogravimetric analyses are conducted with the caffeine hydrate and azithromycin dihydrate; the results are given in Fig. 4B. It is worth noting that during TGA measurement, samples are exposed to continuous dry nitrogen purge as in the DSC, which led to immediate sample weight loss at ambient temperature. The caffeine hydrate is not a robust monohydrate, but rather a 0.8 hydrate or is also classified by some researchers as a non-stoichiometric hydrate [2]. A complete dehydration of the 0.8 hydrate of caffeine would lead to a theoretical weight loss of 6.8%. The TGA of caffeine hydrate shows a weight loss of ~6.6% from 25 °C to 80 °C, in a good agreement with the theoretical weight loss of a complete dehydration. As temperature increases beyond 80 °C, the anhydrous caffeine subsequently undergoes sublimation which is indicated by continuous weight loss until melting occurs.

TGA results of azithromycin dihydrate shows a weight loss of approximately 4.5% between room temperature and melting. This weight loss is in exact agreement with the theoretical weight loss of 4.5% for a complete dehydration of azithromycin dihydrate. This weight loss confirms that azithromycin dihydrate undergoes complete dehydration upon heating and dehydrates to azithromycin anhydrate (instead of the sesquihydrate) prior to melting.

DSC and TGA data are also collected with the anhydrous model compounds, ibuprofen and Compound A. The results show no significant weight loss or thermal events other than melting, typical of what is expected of anhydrous materials. Such data is not shown for brevity since there is no effective change in these macroscopic measurements over the temperature ranges considered by the complementary AFM methods.

While all of the VTPXRD, DSC and TGA data yield dehydration signatures for hydrated samples and are featureless for the anhydrous control specimens, these measurements typically require macroscopic sample quantities of 5–30 mg. Furthermore, the dehydration temperatures identified in this manner are relatively broad and can be dependent on the temperature ramp- rate. In order to identify mechanisms contributing to the apparent breadth of temperatures for dehydration, for instance due to any specimen heterogeneities, it is crucial to develop methods to assess these transitions for smaller volumes.

Therefore, employing AFM-based indentation arrays as described in Figs. 1 and 2, specimens of single API particles with a mass on the order of approximately 100 ng can be investigated. The most frequent modulus detected for such small volumes (the statistical mode for up to 256 distinct measurements in each 16 × 16 indentation map) is plotted in Fig. 5 for all four of the API's, at each temperature considered in steps of 2 or 3 °C. Results for caffeine hydrate upon 8 times stronger loading (1 μN) are also incorporated, revealing a nearly identical response even though the sampled volume is ~16 times larger.

Since ibuprofen does not hydrate, and only has one polymorph, it is an excellent control to show that anhydrous materials do not exhibit a sharp increase in the surface elastic modulus at any temperature before they melt. Over three repeated experiments on single ibuprofen crystals, the modulus mode for ibuprofen remained <25 MPa between room temperature and 70 °C based on 10 °C steps. This consistent response, nearly to the melting temperature of 76 °C, is as expected for anhydrous ibuprofen. For crystalline anhydrous Compound A as well, throughout the thermally featureless temperature range of 30–90 °C, the surface remained consistently compliant with a maximum modulus mode of 15 MPa.

Caffeine hydrate, on the other hand, exhibits a broad dehydration event between 45 and 55 °C as shown above via conventional VTPXRD. Below or above this temperature the modulus mode is approximately 50 MPa or less, whereas at 47 °C, the modulus mode jumps to

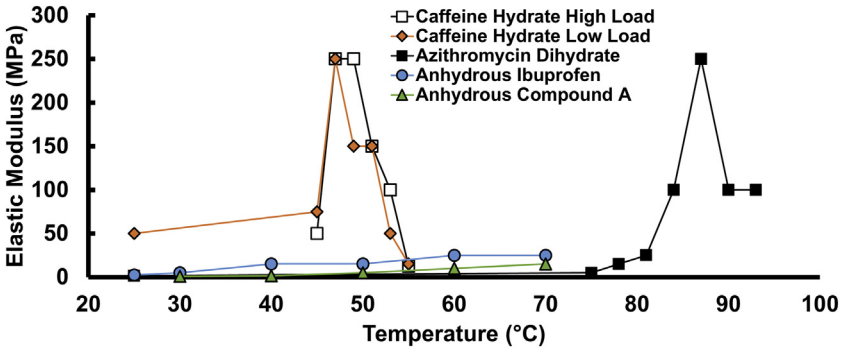

Fig. 5. Summary of modulus modes (peak in modulus histograms as in Fig. 2C), as a function of temperature, for caffeine hydrate with a peak indentation load of 1 μN, and also caffeine hydrate, azithromycin dihydrate, anhydrous ibuprofen, and anhydrous Compound A with peak indentation loads of 125 nN.

250 MPa regardless of indentation load force. Nearly as stiff surfaces are also encountered at 49 °C and 51 °C, but not 45 °C or 53 °C, suggesting local sensitivity to the phase transition within 4 °C above the transition temperature.

Azithromycin, in its dihydrate form, also exhibits signals in VTPXRD, TGA, and DSC indicative of a dehydration event. Compared to that expected between 70 and 100 °C from the macroscopic VTPXRD measurements, the AFM results detect a marked peak in elastic modulus of approximately 250 MPa at 87 °C, with approximate values of 100 MPa or greater between 84 °C and 93 °C and modulus values of <25 MPa below 81 °C. Table 1 summarizes all of these various macroscopic and nanoscale results for the anhydrous and hydrated specimens.

It is noteworthy that these AFM-acquired values seem unexpectedly low, for instance when comparing the caffeine hydrate moduli with published reports obtained via various forms of instrumented indentation techniques [15,16]. Those studies employed peak loads from 600 μN to as high as 250 mN, which are 5 thousand to 2 million times higher than the 125 nN peak loads used for each of the samples reported here. The ~1–3 orders of magnitude difference between these various studies and the present AFM work may result from the different loading conditions, or different sample preparation methods, or the different measurement approaches and calibrations in general. In practice, absolute modulus measurements with AFM are frequently substantially different from those determined with other methods, such that the relative changes in moduli at the dehydration temperature are the most significant AFM-based finding.

This result implies that AFM indentations may serve as a reasonable diagnostic test of the hydration state for single sub-micron sized crystals. The volume sampled above or below the dehydration temperature, when the specimen is relatively compliant, can be conservatively estimated as <0.0013 μm^3 or 0.0033 μm^3 for the caffeine and azithromycin respectively. This volume is shaped as a half-oblate spheroid, with a diameter established by the probe contact radius and a depth established by the probe indentation depth. According to Hertzian contact mechanics, these amount to –contact radii of 167–211 nm and a peak indentation depth of 11–18 nm, respectively, given the 50 or 25 MPa bulk moduli for the two specimens, 2.5 μm radius spherical silica glass probe, and peak applied force of 125 nN. At or near the dehydration temperature for caffeine and azithromycin, however, when the modulus jumps by a factor of ~5-10, the indentation depth for instance for caffeine decreases to only 4 nm and contact radius drops to 98 nm. The corresponding volume then diminishes to just 0.000154 μm^3, roughly 10 times smaller than away from the dehydration temperatures. As a result, truly nanoscale measurements of dehydration phenomena, laterally and with respect to specimen depth and overall sample volume, become accessible with this approach.

At the same time, the apparent stiffening at dehydration temperatures may seem counterintuitive. It may result from several possible convoluting effects common to indentation-based mechanical measurements, including changes in the modulus for the distinct polymorphs, variations in adhesion between probe and sample, and the spatial and temporal evolution of the transformation which is macroscopically distributed over a range of temperatures, times, lateral positions, and depths. But since the measured modulus rises to a peak at the dehydration temperature, and falls beyond it instead of exhibiting a step function, then distinct mechanical properties for the hydrated and dehydrated polymorphs cannot explain the observed results. And since the results are highly repeatable as well as correspond to well-understood macroscopic indicators of dehydration events, spatial and temporal variations also cannot explain the observed modulus enhancements.

It is possible that adhesion forces may affect the modulus detected at each temperature examined. Adhesion is related to the relative surface energies between the probe apex and the particle surface, possibly mediated by the presence of water which of course is especially likely to be present, and poorly bound only near a dehydration temperature. Adhesion forces may be measured by AFM based on the most attractive force either during tip-approach (upon jump to contact) or upon retraction after contact during indentation (snap-off). The adhesion energy can also be recorded, based on the difference in forces between the initial path of the tip when it begins to interact with and indent the sample (solid lines in Fig. 1B) and the return path of the tip as it leaves the surface (dotted lines). Fig. 6 displays results from the most common approach, i.e. the force required to rupture the adhesion between the AFM probe and surface. Elastic modulus mode values as in Fig. 5 are also overlain, all as a function of temperature for the caffeine hydrate as it transitions to the dehydrated state. These results correspond to low load indentation measurements (125 nN peak force), with

Table 1
Summary of dehydration events resolved conventionally (macroscopically) and via AFM indentations for two hydrated specimens, caffeine and azithromycin, as well as 2 anhydrous controls, ibuprofen and Compound A.

Technique	Sample mass	Caffeine Hydrate	Azithromycin dihydrate	Ibuprofen	Compound A
VTXRD	15–30 mg	45°C–55 °C	70 °C–100 °C	N/A	N/A
DSC	3–5 mg	25°C-80°C	25°C–75 °C	N/A	N/A
AFM	10–100 ng, single crystal	47 °C (±4 °C)	87 °C (±6 °C)	N/A	N/A
AFM modulus: non-dehydration temperatures)	N/A	~50 MPa	~25 MPa	~15 MPa	~10 MPa
AFM modulus: at dehydration events	N/A	~250 MPa	~250 MPa	N/A	N/A

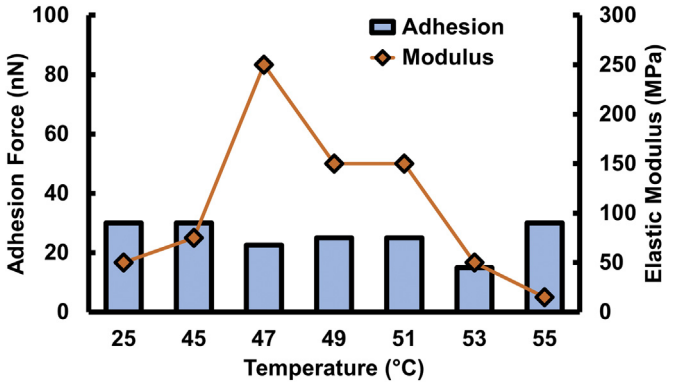

Fig. 6. Statistical mode for adhesion force (bars) and modulus (line plot) as a function of temperature for caffeine hydrate with peak indentation loads of 125 nN.

qualitatively equivalent results also detected upon high load (1 μN) indentations. Clearly, the adhesion force does not vary significantly as a function of temperature, suggesting that free water at the surface and/or capillary action only negligibly influence the temperature dependent modulus results. Measurements as a function of time over several or tens of minutes are generally uniform, consistent with dehydration times on the order of tens of minutes according to powder x-ray diffraction measurements of more bulk-like quantities of identical caffeine crystals. It must be considered, however, that extensions of this approach could reveal local variations in the kinetics of the dehydration process, for instance due to local microstructural variations such as surface facet orientations, grain sizes, or phase purity.

Although surface water is not directly implicated in the apparent surface stiffening, the increased modulus specifically at dehydration temperatures may indicate that the enhanced mobility of near- and sub- surface water molecules, loosely bound at these temperatures, collectively can accommodate substantial amounts of energy during indentation. For lower temperatures these molecules are bound to the crystal, while they are no longer present at higher temperatures. This effect may be further enhanced by water molecule ordering and/or layering at the surface [17,18], which would contribute to an increased stiffness or energy dissipation mechanism especially given the inherent nanoconfined hydration channels present in the single crystal hydrates studied herein. Again, this would vary strongly with the temperature-dependent presence of water inherent to the dehydration event.

4. Conclusions

Temperature-induced dehydration phenomena have been investigated using AFM nanoindentation. Caffeine hydrate and azithromycin dihydrate are model compounds, along with ibuprofen and a proprietary Compound A as anhydrous (negative) controls. Temperature dependent increases in the mechanical modulus detected at the nanoscale, for single crystals of the hydrated compounds only, correspond to dehydration events measured conventionally for macroscopic volumes of their powders. No change in modulus is observed with temperature for the anhydrous compounds. This research thus confirms that AFM is capable of identifying temperature-induced dehydration events for pharmaceutical materials using sample volumes that are orders of magnitude smaller than conventional approaches such as DSC, TGA, and VTPXRD. As with many AFM-based mechanical measurements, the consistent absolute values for the measured moduli are notably lower than other mechanical studies which employed 3–6 orders of magnitude larger forces, such that the AFM-sampled volumes are thousands to millions of times smaller. Nevertheless, the relative changes in modulus with temperature (>10× higher at the transition temperature) are a noteworthy new approach for investigating dehydration temperatures at very early stages of pharmaceutical development, especially when material supplies or costs are limited. Spatial heterogeneities in dehydration events for phase separated drug formulations, or perhaps even kinetics investigations for instance as a function of crystal facet, can also be directly considered in the future due to the imaging capability and nanoscale lateral resolution of the technique. More broadly, dehydration studies are therefore feasible for a range of high value or limited supply materials systems beyond drug discovery, for instance biomedical specimens, combinatorial polymers synthesis, archeological studies, or art restoration [19,20].

Acknowledgements

K. Atamanuk recognizes Pfizer Inc. for project support. For W. Linthicum, research reported in this publication was supported by the National Institute Of Arthritis And Musculoskeletal And Skin Diseases of the National Institutes of Health under Award Number R01AR073206, USA. The content is solely the responsibility of the authors and does not necessarily represent the official views of the National Institutes of Health. B. D. Huey acknowledges NSF:MRI Development Grant 1726862, USA.

W. Yu, M. C. Thomas, and R. C. Wadams thank Bruno Hancock, Brian Samas, and Doug Dickey for their guidance and support.

References

[1] P. Sundaramurthi, R. Suryanarayanan, Azithromycin hydrates—implications of processing-induced phase transformations, J. Pharm. Sci. 103 (2014) 3095–3106.
[2] H. Bothe, H. Cammenga, Composition, properties, stability and thermal dehydration of crystalline caffeine hydrate, Thermochim. Acta 40 (1980) 29–39.
[3] S.R. Vippagunta, H.G. Brittain, D.J.W. Grant, Crystalline Solids, Adv. Drug Deliv. Rev. 48 (2001) 3–26.
[4] B.C. Hancock, G. Zografi, Characteristics and significance of the amorphous state in pharmaceutical systems, J. Pharm. Sci. 86 (1997) 1–12.
[5] J.F. Kryzaniak, G.R. Williams, N. Ni, Identification of phase boundaries in anhydrate/hydrate systems, J. Pharm. Sci. 96 (2007) 1270–1281.
[6] B.D. Huey, J. Luria, D.A. Bonnell, Scanning probe microscopy in materials science, in: P. Hawkes, J.C.H. Spence (Eds.), Springer Handbook of Microscopy, Springer-Verlag, New York, 2018.
[7] R. Ferencz, J. Sanchez, B. Blümich, W. Herrmann, AFM nanoindentation to determine Young's modulus for different EPDM elastomers, Polym. Test. 31 (2012) 425–432.
[8] L. Saad, Americans' Coffee Consumption Is Steady, Few Want to Cut Back, Gallup, Jul 29, 2015.
[9] j.-r Authelin, Thermodynamics of non-stoichiometric pharmaceutical hydrates, Int. J. Pharm. 303 (2005) 37–53.
[10] J.E. Sader, I. Larson, P. Mulvaney, L.R. White, Method for the calibration of atomic force microscope cantilevers, Rev. Sci. Instrum. 66 (1995) 3789–3798.
[11] M.F. Doerner, W.D. Nix, A method for interpreting the data from depth-sensing indentation instruments, J. Mater. Res. 1 (1986) 601–609.
[12] S. Liu, Q. Wang, Determination of Young's modulus and Poisson's ratio for coatings, Surf. Coat. Technol. 201 (2007) 6470–6477.
[13] J.S. González-González, O. Zúñiga-Lemus, M.D.C. Hernández-Galindo, Hydrated solid forms of theophylline and caffeine obtained by Mechanochemistry, ISOR J. Pharm Biol Sci. 7 (2017) 28–30.
[14] J. Pirttimäki, E. Laine, J. Ketolainen, P. Paronen, Effects of grinding and compression on crystal structure of anhydrous caffeine, Int. J. Pharm. 95 (1993) 93–99.
[15] R.J. Roberts, R.C. Rowe, The relationship between Young's modulus of elasticity of organic solids and their molecular structure, Powder Technol. 65 (1991) 139–146.
[16] S. Ghosh, A. Mondal, M.S.R.N. Kiran, U. Ramamurty, C.M. Reddy, The role of weak interactions in the phase transition and distinct mechanical behavior of two structurally similar caffeine co-crystal polymorphs studied by Nanoindentation, Cryst. Growth Des. 13 (10) (2013) 4435–4441.
[17] S. Jeffery, P.M. Hoffmann, J.B. Pethica, C. Ramanujan, H.Ö. Özer, A. Oral, Direct measurement of molecular stiffness and damping in confined water layers, Phys. Rev. B 70 (5) (2004), 054114.
[18] B. Kim, S. Kwon, H. Mun, S. An, W. Jhe, Energy dissipation of nanoconfined hydration layer: long-range hydration on the hydrophilic solid surface, Sci. Rep. 4 (2014) 6499.
[19] S. Struever, Flotation Techniques for the Recovery of Small-Scale Archaeological Remains, vol. 33, Cambridge University Press, 1968 353–362.
[20] R. Klockenkämper, A. von Bohle, L. Moens, Analysis of pigments and inks on oil paintings and historical manuscripts using total reflection x-ray fluorescence spectrometry, X-Ray Spectrom. 29 (2000).